ELSEVIER

Journal of Alloys and Compounds 437 (2007) 102–106

Journal of ALLOYS AND COMPOUNDS

www.elsevier.com/locate/jallcom

Thermodynamic assessment of the Ce–Mn system

Chengying Tang, Yong Du *, Lijun Zhang, Honghui Xu, Zhijun Zhu

State Key Laboratory of Powder Metallurgy, Central South University, Changsha, Hunan 410083, China

Received 15 June 2006; received in revised form 14 July 2006; accepted 18 July 2006
Available online 23 August 2006

Abstract

The binary Ce–Mn system is investigated via key experiments and thermodynamic modeling. The phase diagram data available in the literature are critically reviewed. Four key alloys are prepared by arc melting the pure elements, annealed at 600 °C for 8 days and then subjected to X-ray diffraction (XRD) analysis for phase identification and to differential thermal analysis (DTA) for measurement of phase transition temperatures. The thermodynamic optimization of the Ce–Mn system is performed by considering the experimental data from the literature and the present work. A consistent thermodynamic data set for the Ce–Mn system is obtained by optimization of the selected experimental data. The calculated phase diagram agrees well with the experimental data.

Keywords: Ce–Mn system; Phase diagram; Thermodynamic modeling; X-ray diffraction; Thermal analysis

1. Introduction

Al-based alloys with nonperiodic structure such as amorphous and icosahedral phases are attractive materials due to favorable properties of high-strength and lightweight. The Ce–Mn system is a sub-binary system in multi-component Al-based alloys containing nanoscale quasicrystalline particles [1,2]. Rapidly solidified nano-icosahedral reinforced Al–Ce–Mn alloys have attractive properties such as good bending ductility and high tensile strength up to 1320 MPa [1]. The specific strength of rapidly solidified $Al_{93}Mn_5Ce_1Ni_1$ (at.%) alloy is evaluated to be as high as 3.9×10^5 Nm kg^{-1}, which is considerably higher than the highest value (3.6×10^5 Nm kg^{-1}) of the Al-based amorphous single phase and three times higher than that for the conventional Al-based crystalline alloy (7075-T6) [2]. Amorphous $Ce_{100-x}Mn_x$ alloys ($x = 20$–80 at.%) with high glass-forming ability can be fabricated by a direct current (dc) high-rate sputtering technique [3]. Knowledge of the phase equilibria is of fundamental importance to predict the glass-forming region. A thorough thermodynamic assessment of the Ce–Mn system is necessary to perform thermodynamic extrapolations to the related higher order systems. The purpose of this work is to develop a self-consistent set of thermodynamic parameters for the Ce–Mn system by key experiments and thermodynamic modeling.

2. Evaluation of experimental data

The first investigation of the Ce–Mn system was carried out by Rolla and Iandelli [4], who found a narrower miscibility gap for the liquid than that in the La-Mn system. Subsequently, Iandelli [5] determined the complete phase diagram with the alloys made from 99.5 wt.% Ce and 99.8 wt.% Mn, and suggested the existence of the miscibility gap between 68 at.% and 82 at.% Mn on the basis of the thermal analysis measurements. However, the existence of the miscibility gap was not confirmed by Mirgalovskaya and Strel'nikova [6], who reinvestigated the phase relations in the Ce–Mn system using a combination approach of thermal analysis and metallography. Their experimental results [6] agrees reasonably with those of Iandelli [5] in the composition range from pure Ce to 40 wt.% Mn within experimental uncertainty, except for the eutectic reaction: Liquid → (γCe) + (αMn), which was determined to occur at 612 °C and 15.1 at.% Mn by Iandelli [5], at 635 °C and about 12 at.% Mn by Mirgalovskaya and Strel'nikova [6], respectively.

The major discrepancy among the literature data [4–6] is if there is a miscibility gap for the liquid phase. Iandelli [5] claimed that the flat liquidus in the composition range of 68–82 at.% Mn

* Corresponding author. Tel.: +86 731 8836213; fax: +86 731 8710855.
E-mail addresses: yong-du@mail.csu.edu.cn, csutcy@163.com (Y. Du).

0925-8388/$ – see front matter © 2006 Elsevier B.V. All rights reserved.
doi:10.1016/j.jallcom.2006.07.071

is associated with the occurrence of liquid miscibility gap, while Mirgalovskaya and Strel'nikova [6] attributed the flat liquidus to be due to an anomalous behavior of the alloys resulting from the decomposition of (γMn) to (βMn). Using scanning electron microscopy (SEM) with energy dispersive X-ray analysis (EDX) and X-ray diffraction (XRD) technique, Tang et al. [7] concluded that no liquid miscibility gap exists in the Ce–Mn system. The liquidus data and invariant reactions at 998 °C and 1087 °C [6] are considered reliable and, therefore, utilized in the present modeling. The liquidus data of Iandelli [5] are also used in the present assessment. The monotectic reaction, Liquid 2 → Liquid 1 + (βMn), has not been considered in the present optimization.

By means of differential thermal analysis (DTA), metallography and X-ray diffraction technique, the phase relation in Ce-rich region below 20 at.% Mn was determined by Thamer [8] using starting materials with the purities of 99.8 at.% Ce and 99.96 at.% Mn. The eutectic reaction: Liquid → (γCe) + (αMn) was determined to be at 16.1 ± 0.5 at.% Mn and 622 °C [8]. The catatectic reaction: (δCe) → (γCe) + Liquid, in the Ce-rich side was determined to occur at 5 ± 1 at.% Mn and 638 °C [8]. Another invariant reaction, catatectic reaction: (βMn) → (αMn) + Liquid, was reported to exist at 625 °C. Compared with the previous investigation [4–6], Thamer [8] employed the starting materials with higher purities. As a consequence, the experimental data of Thamer [8] in Ce-side are considered to be reliable and used in the present optimization.

By measuring the density of an alloy containing 6.4 wt.% Mn from room temperature to 800 °C, the eutectic in the Ce–Mn system was reported by Perkins to be 14 at.% Mn and 618 ± 3 °C. The eutectic point reported by Perkins et al. [9] agrees with that from Thamer [8].

The solubilities of Mn in (δCe) and (γCe) were determined to be 5 at.% and 2 at.% Mn at 638 °C by Thamer [8], respectively. The solubility for Mn in (γCe) drops to less than 1 at.% at 600 °C [8]. By examining lattice parameters, Iandelli [5] found that (αMn) dissolves negligible amount of Ce at room temperature. The solubility of Ce in (βMn) was determined to be 1.8 at.% Ce by Tang [7].

No thermodynamic data for the Ce–Mn system are available. Based on early phase diagram data [4–6], the Ce–Mn system was reviewed by several groups of authors [10–19].

3. Experimental procedure

In the present work, four alloys ($Ce_{90}Mn_{10}$, $Ce_{78}Mn_{22}$, $Ce_{61}Mn_{39}$, $Ce_{48}Mn_{52}$ in at.%) were prepared in order to provide reliable phase diagram data in Ce-rich side of the Ce–Mn system. The choice of the compositions of the decisive alloy is guided by the assessed phase diagram [19]. The starting materials are Ce-rods (purity: 99.9 mass%) and Mn-pieces (purity: 99.9 mass%). The surface of Ce-rods were ground, polished, cleaned by ethanol and acetone and then kept in acetone before use. Mn pieces were treated with nitric acid to remove the surface oxides, washed sequentially with water, ethanol and acetone, and kept in acetone for use. The alloys with the masses of about 2.5 g were prepared with arc melting furnace under argon (purity: 99.999%; additionally purified by Ti-gettering) on a copper hearth using a nonconsumable tungsten electrode. No chemical analysis for the alloys was conducted since the mass loss during arc melting was generally less than 1%. The as-cast alloys were sealed in evacuated silica tubes under vacuum and annealed at 600 °C for 8 days in high-temperature diffusion furnace (L-45-1-135, QingDao, China).

Phase identification was carried out by XRD with monochromatic Cu Kα (Rigaku D/max2550VB, Japan). DTA (DSC404C, NETZSCH, Germany) measurements of annealed alloys were carried out in Al_2O_3 crucibles under a flow of pure Ar atmosphere. The measurement was performed between room temperature and 1000 °C with a heating and cooling rate of 5 °C/min. In the temperature range examined, the accuracy of the temperature measurement was estimated to be ±2 °C. The invariant reaction temperatures were determined from the onset of the thermal effect during the heating step, and the offset of last thermal effect on heating was taken for the liquidus.

4. Thermodynamic model

4.1. Unary phases

The Gibbs energy function ${}^0G_i^\Phi(T) = G_i^\Phi(T) - H_i^{SER}$ for the element i (i = Ce, Mn) in the phase Φ (Φ = liquid, δ(Mn, Ni), γ(Mn, Ni)) is expressed by an equation of the form:

$$ {}^0G_i^\Phi(T) = a + bT + cT\ln T + dT^2 + eT^{-1} + fT^3 + gT^7 + hT^{-9} \quad (1) $$

where H_i^{SER} is the molar enthalpy of the element i at 298.15 K and 1 bar in its standard element reference (SER) state, and T is the absolute temperature. The last two terms in Eq. (1) are used only outside the ranges of stability [20], the term gT^7 for a liquid below the melting point, and hT^{-9} for solid phases above the melting point. In the present work, the Gibbs energy functions for Ce and Mn are from the SGTE compilation by Dinsdale [21].

4.2. Solution phases

In the Ce–Mn system, there are five solution phases: liquid, δ(Mn, Ni), γ(Mn, Ni), (βMn) and (αMn). The Gibbs energy for liquid is expressed as follows:

$$ G_m^L - H^{SER} = x_{Ce}\,{}^0G_{Ce}^L + x_{Mn}\,{}^0G_{Mn}^L + RT[x_{Ce}\ln x_{Ce} + x_{Mn}\ln x_{Mn}] + {}^EG_m^L \quad (2) $$

where H^{SER} is the abbreviation of $x_{Ce}H_{Ce}^{SER} + x_{Mn}H_{Mn}^{SER}$, R the gas constant, and the x_{Ce} and x_{Mn} are the mole fractions of Ce and Mn, respectively. The ${}^EG_m^L$ is the excess Gibbs energy. It is described by the Redlich–Kister polynomials [22],

$$ {}^EG_m^L = x_{Ce}x_{Mn}\sum_i {}^iL_{Ce,Mn}^L(x_{Ce} - x_{Mn})^i \quad (3) $$

where ${}^iL_{Ce,Mn}^L$ is the interaction parameter between elements Ce and Mn, which is to be optimized in the present work. Its general form is ${}^iL_{Ce,Mn}^L = a_i + b_iT$.

The Gibbs energies of δ(Mn, Ni), γ(Mn, Ni), and (αMn) phases are modeled as a sum of a nonmagnetic contribution (${}^0G^{nmg}$) and a magnetic one (ΔG^{mg}), with the nonmagnetic part described by Eq. (2) and the magnetic part by the Hillert–Jarl–Inden model [23]. The concentration dependence of magnetic ordering temperature T_C and magnetic moment β can be described as:

$$ T_C^\Phi = x_{Ce}\,{}^0T_{CCe}^\Phi + x_{Mn}\,{}^0T_{CMn}^\Phi + x_{Ce}x_{Mn}T_{Ci,j}^\Phi \quad (4) $$

$$ \beta^\Phi = x_{Ce}\,{}^0\beta_{Ce}^\Phi + x_{Mn}\,{}^0\beta_{Mn}^\Phi + x_{Ce}x_{Mn}L_\beta^\Phi \quad (5) $$

where ${}^0T_{Ci}^{\Phi}$ and β_i^{Φ} correspond to pure elements i, and are taken from the SGTE compilation by Dinsdale [21]. Owing to low solubility and lack of experiment data, magnetic parameters $T_{Ci,j}^{\Phi}$ and L_{β}^{Φ} were set to zero.

5. Results and discussion

XRD examination on the prepared alloys verified that there is no compound in the Ce–Mn system. Invariant reaction temperatures derived from DTA measurement on annealed alloys are listed in Table 1 and also presented in Fig. 1. As shown in Table 1, the present experimental data agree well with the accepted ones in the literature. The thermodynamic parameters are optimized by means of the PARROT module of Thermo-Calc software package [24]. The step-by-step optimization procedure carefully described by Du et al. [25] was utilized in the present assessment. In the optimization procedure, each piece of experimental information is given a certain weight. The weights were changed systematically during the assessment until most of the experimental data were reproduced within the expected uncertainty limits.

Since there is no thermodynamic data available in the literature, the parameters for liquid, a_0 and b_0 in Eq. (3) are adjusted to reproduce Ce-rich or Mn-rich partial liquidus and related catatectic reaction at 638 °C or 1087 °C. The obtained parameters were used as starting value for subsequent optimizations. In the present work, it was found that the introduction of further parameters, a_1 and a_2, can improve the description of the liquid phase.

(δCe) and (δMn) was treated as one phase δ(Ce, Mn). Considering the reaction: δ(Ce, Mn) → γ(Ce, Mn) + Liquid, two parameters, $a_0^{\delta(Ce,Mn)}$ and $a_1^{\delta(Ce,Mn)}$, were introduced to describe the δ(Ce, Mn) phase. An analogous treatment was applied to γ(Ce, Mn) phase, Two parameters, $a_0^{\gamma(Ce,Mn)}$ and $a_1^{\gamma(Ce,Mn)}$ were thus adjusted for the description of γ(Ce, Mn) phase. In the present modeling, (βMn) was described by one sublattice (Mn, Ce). Since no lattice stability for Ce in the beta-Mn structure is available in the literature, the Gibbs energy of Ce in (βMn) structure is assessed to be 2500 relative to the stable structure of (γCe) (i.e., ${}^0G^{\beta Ce} = 2500 + {}^0G^{\gamma Ce}$). The temperature-dependent regular parameter was then adjusted for (βMn) in view of its stability within a wide temperature range.

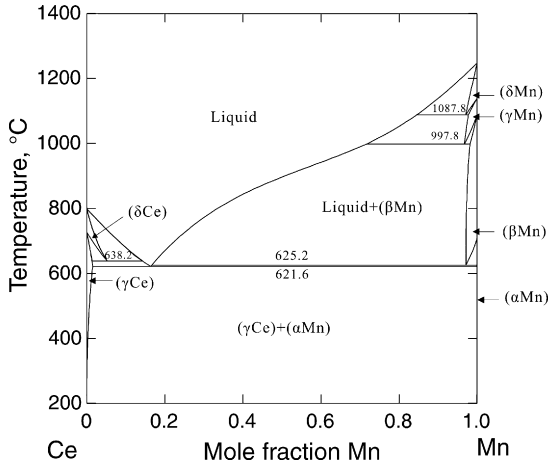

Fig. 1. Calculated Ce–Mn phase diagram in the present work.

In view of the negligible solubility for Ce in (αMn) [5], no thermodynamic parameter for this phase was introduced in the present work.

The finally optimized thermodynamic parameters for the Ce–Mn binary system are presented in Table 2. The calculated phase diagram using the present parameters is shown in Fig. 1. Fig. 2 compares the computed phase diagram along with the experimental data. Calculated temperatures and compositions for invariant equilibria in the Ce–Mn system are listed in Table 1 along with the experimental ones. As shown in the table and figures, an excellent agreement is obtained between the calculations and experiments from the literature and present work. The presently calculated Ce–Mn phase diagram is verified to be a really stable one with Pandat program [26]. By using the presently obtained thermodynamic parameters for the Ce–Mn system, the thermodynamic parameters for the Al–Ce [27] and that for the Al–Mn [28] system, Tang et al. [29] has calculated the phase relation of the Al–Ce–Mn system successfully. It is

Table 1
Comparison between the measured and calculated invariant equilibria

Equilibrium	Composition (at.% Mn)			T (°C)	Method	Source
Liquid ↔ (γCe) + (αMn)	16.1	~2.0	~99.5	622 ± 2	DTA, XRD	[8]
	16.35	1.53	100.0	621.6	Calculated	This work
				621 ± 2	DTA	This work
(δCe) ↔ (γCe) + Liquid	14.0	5.0	2.0	638 ± 2	DTA, XRD	[8]
	14.30	5.25	1.36	638.2	Calculated	This work
				640 ± 2	DTA	This work
(βMn) ↔ (αMn) + Liquid	~98.0	~99.5	~16.3	625 ± 2	DTA, EDX	[7,8]
	97.19	100.0	16.63	625.2	Calculated	This work
(γMn) ↔ (βMn) + Liquid	~98.0	~99.0	~71.0	998 ± 2	TA	[5,6]
	96.76	98.19	71.74	997.8	Calculated	This work
(δMn) ↔ (γMn) + Liquid	~98.0	~98.3	~86.0	1087 ± 2	TA	[6]
	97.12	97.79	84.61	1087.8	Calculated	This work

Table 2
Optimized thermodynamic parameters of the Ce–Mn System[a]

Liquid: $(Ce, Mn)_1$
$^0L^{L}_{Ce,Mn} = 15584.7 - 5.30258T$
$^1L^{L}_{Ce,Mn} = -2736.1$
$^2L^{L}_{Ce,Mn} = -1532.3$

δ(Ce, Mn): $(Ce, Mn)_1$
$^0L^{\delta(Ce,Mn)} = 23607.2$
$^1L^{\delta(Ce,Mn)} = -2250.0$

γ(Ce, Mn): $(Ce, Mn)_1$
$^0L^{\gamma(Ce,Mn)} = 29193.0$
$^1L^{\gamma(Ce,Mn)} = 2006.6$

βMn: $(Ce, Mn)_1$
$^0L^{\beta Mn} = 13261.4 + 13.54757T$
$^0G^{\beta Ce} = 2500 + {}^0G^{\gamma Ce}$

[a] Temperatures (T) in Kelvin and Gibbs energy in J/mol of atoms unit.

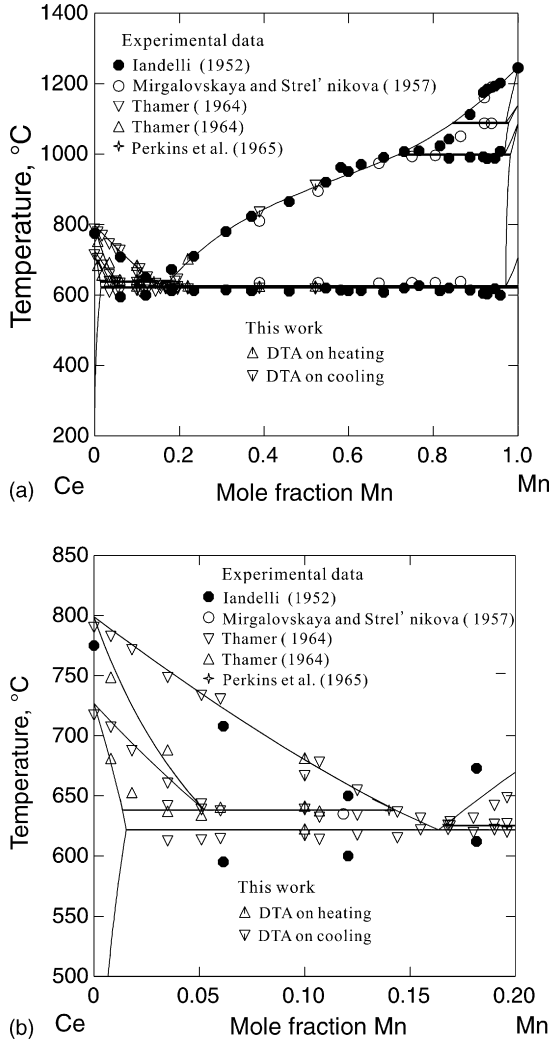

Fig. 2. Calculated Ce–Mn phase diagram with the present experimental data as well as the experimental data from the literature [5,6,8,9], (a) in whole composition range and (b) in the range of 0–20 at.% Mn.

expected that the presently obtained thermodynamic parameters for the Ce–Mn system can be used for the optimization of related ternary and multi-component system.

6. Conclusions

The Ce–Mn system has been investigated via thermodynamic modeling, supplemented with key experiment. A self-consistent set of thermodynamic parameters has been obtained by considering the present experiment as well as critically evaluated literature data. The calculated phase diagram agrees well with the experimental one.

Acknowledgements

The financial support from National Natural Science Foundation of China (Grant No. 50571114) and National Outstanding Youth Science Foundation of China (Grant No. 50425103) is greatly acknowledged. One of the authors (Yong Du) acknowledges Furong Chair Professorship Program released by Hunan Province of PR China for financial support.

References

[1] A. Inoue, M. Watanabe, H.M. Kimura, F. Takahashi, A. Nagata, T. Masumoto, Mater. Trans. JIM. 33 (1992) 723–729.
[2] H.M. Kimura, K. Sasamori, M. Watanabe, A. Inoue, T. Masumoto, Mater. Sci. Eng. A 181/182 (1994) 845–849.
[3] Y. Obi, S. Murayamab, Y. Amakaib, K. Asano, Physica B 359–361 (2005) 299–301.
[4] L. Rolla, A. Iandelli, Ber. Deut. Chem. Ges. 75 (1942) 2091–2095.
[5] A. Iandelli, Lincei-Rend. Sc. fis. mat. e nat. 13 (1952) 265–268.
[6] M.S. Mirgalovskaya, I.A. Strel'nikova, Trans. Inst. Met. Akad. Nauk SSSR 2 (1957) 135–138.
[7] C.Y. Tang, Y. Du, H.H. Xu, S.M Hao, L.J. Zhang, Z.J. Zhu, Mater. Lett., under review.
[8] B.J. Thamer, J Less-Common Met. 7 (1964) 341–346.
[9] R.H. Perkins, L.A. Geoffrion, J.C. Biery, Metall. Trans. AIME 233 (1965) 1703–1710.
[10] K.A. Gschneidner Jr., Rare Earth Alloys, Van Nostrand, New York, 1961, pp. 215–217.
[11] M. Hansen, K. Aanderko, Constitution of Binary Alloys, McGraw-Hill, New York, 1958, pp. 503–506.
[12] D.F. Anthrop, U.S. Atom. Energy Comm. UCRL-50315, 1967.
[13] K.A. Gschneider Jr., M.E. Verkade, Document IS-RIC-7, 1974, pp. 26–27.
[14] W.G. Moffatt, Handbook of Binary Phase Diagrams, Genium Publishing Corporation., Schenectady, New York, 1981.
[15] F.A. Shunk, Constitution of Binary Alloys, second supplement, McGraw-Hill, New York, 1969.
[16] R.P. Elliott, Constitution of Binary Alloys, first supplement, McGraw-Hill, New York, 1965, pp. 302–303.
[17] B. Predel, Landolt-Bönstein, New Series, Group IV: Physical Chemistry: Phase Equilibria, Crystallograpic and Thermodynamic Data of Binary Alloys, vol. 5(C), 1993, p. 1.
[18] T.B. Massalski, P.R. Subramanian, H. Okamoto, L. Kacprzak, Binary Alloy Phase Diagrams, vol. 1, ASM International, Metals Park, Ohio, 1990, p. 724.
[19] A. Palenzona, S. Cirafici, J Phase Equilib. 17 (1) (1996) 53–56.
[20] J.O. Andersson, A.F. Guillermet, P. Gustafson, M. Hillert, B. Jansson, B. Sunderman, J. Ågren, Calphad 11 (1987) 93–98.
[21] A.T. Dinsdale, Calphad 15 (4) (1991) 317–425.
[22] O. Redlich, A.T. Kister, Ind. Eng. Chem. 40 (1948) 345–348.
[23] M. Hillert, M. Jarl, Calphad 2 (1978) 227–238.

[24] B. Sundman, B. Jansson, J.O. Andersson, Calphad 9 (1985) 153–190.
[25] Y. Du, R. Schmid-Fetzer, H. Ohtani, Z. Metallkd. 88 (1997) 545–556.
[26] Pandat—Phase diagram Calculation Engine for Multicomponent System, CompuTherm LLC, 437 S. Yellowstone Dr., Suite 217, Madison, WI, 2000.
[27] M.C. Gao, N. Ünlü, G.J. Shiflet, M. Mihalkovic, M. Widom, Metall. Mater. Trans. A 36A (2005) 3269–3279.
[28] Y. Du, J.C. Schuster, Acta Mater., submitted for publication (2006).
[29] C.Y. Tang, Y. Du, H.H. Xu, L.J. Zhang, unpublished results.